Electronic Supplementary Information

Quantifying signal changes in nano-wire based biosensors

Luca De Vico, Martin H. Sørensen, Lars Iversen, David M. Rogers, Brian S. Sørensen, Mads Brandbyge, Jesper Nygård, Karen L. Martinez and Jan H. Jensen

The base conductance G_0 of a cylindrical nano-wire can be computed as:

$$G_0 = \frac{\pi R^2 e\,(n_0\,\mu_n + p_0\,\mu_p)}{L} \tag{12}$$

In case of p-type doped nano-wire it can be semplified as:

$$G_0 = \frac{\pi R^2 e\,p_0\,\mu}{L} \tag{13}$$

where the mobility is simply indicated as μ, as usually reported.

Fig. 1S Signal sensitivity of the **GEN** setup with respect to various experimentally modifiable parameters of Equations (2), (1) and (3) of section 2.2: the nano-wire. The conductance sensitivity of the simulated nano-wire is computed for 100 intervals in the range $\pm 20\%$ of the values of Table 1 for each parameter, and the entire **ENS** is reported against the a) nano-wire radius R, b) the nano-wire oxide layer thickness ΔR, c) the nano-wire permittivity ε_1, d) the nano-wire oxide layer permittivity ε_2. In each graph (a-d) the majority of the **ENS** points are located, logically, at the central value, and constitutes the vertical part of the graphs. In all calculations the charge density is kept fixed $\sigma_b \approx -1.366\text{E}^{-2}$ C m^{-2}.

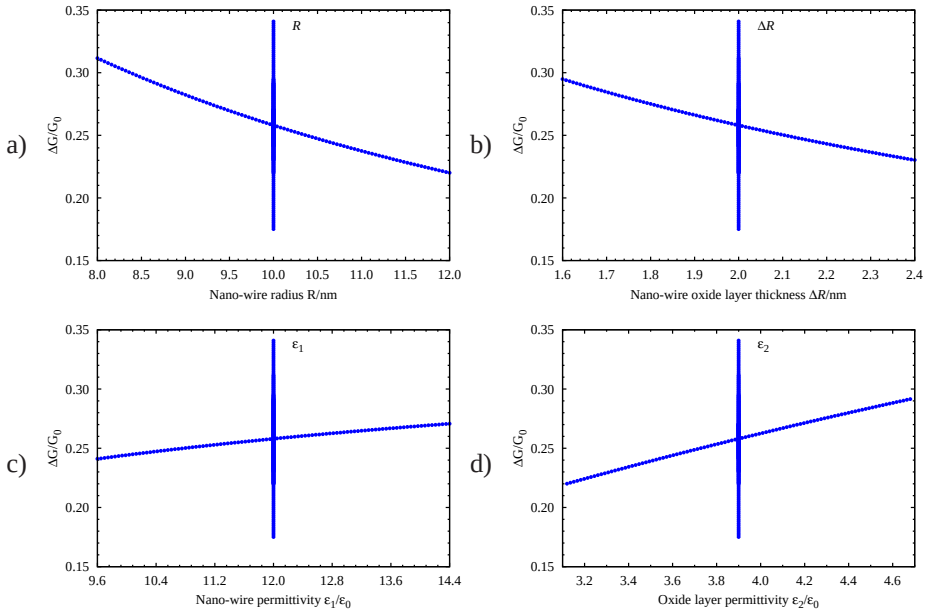

Fig. 2S Signal sensitivity of the **GEN** setup with respect to the buffer Debye length λ_D. The Debye length is varied between a) 0-10 nm and b) 0-100 nm. In all calculations the charge density is kept fixed $\sigma_b \approx -1.366\text{E}^{-2}$ C m^{-2}.

a)

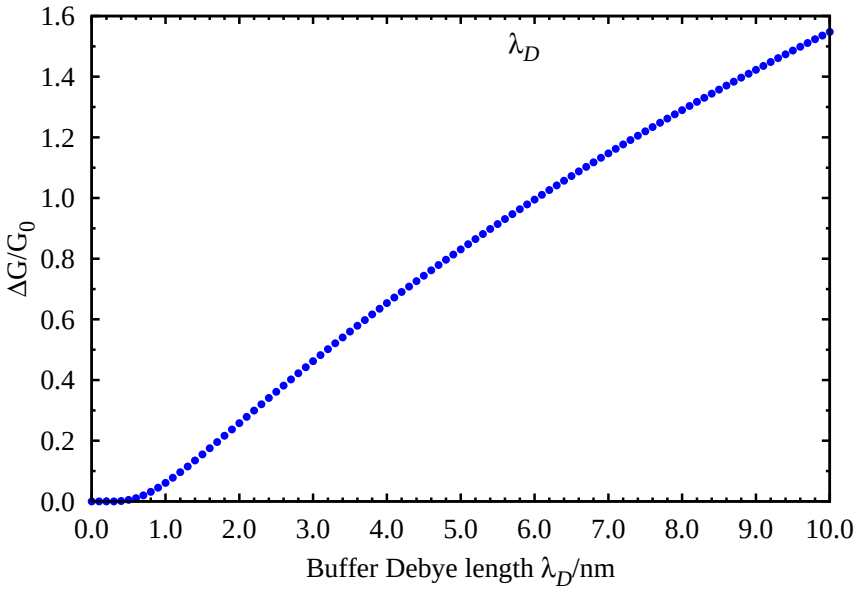

b)

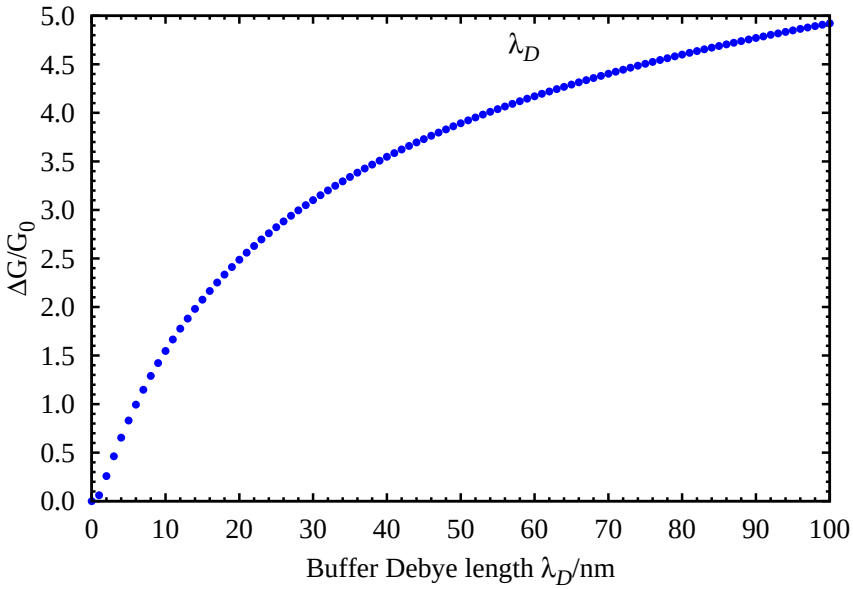

Fig. 3S Figure 3a of Ref. 26, with a superimposed grid, in order to extract experimental data.

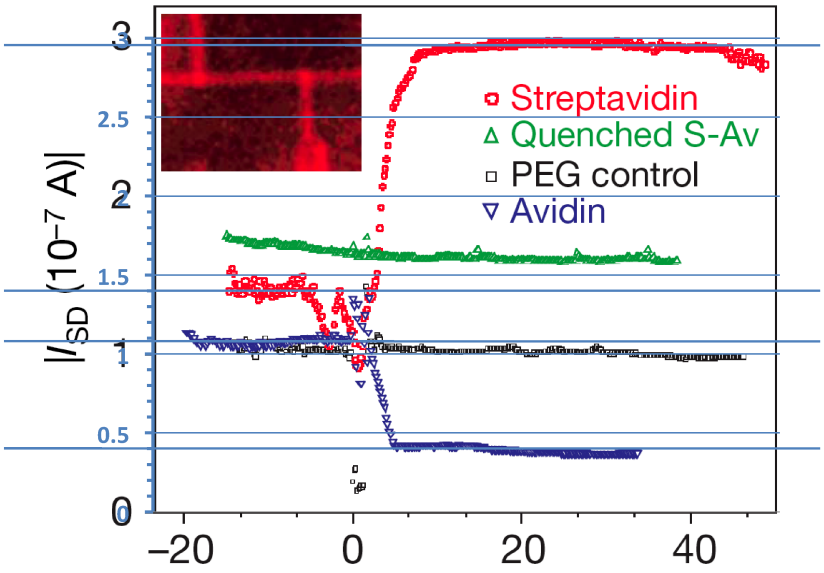

Fig. 4S Figure 3c of Ref. 26, with a superimposed grid, in order to extract experimental data.

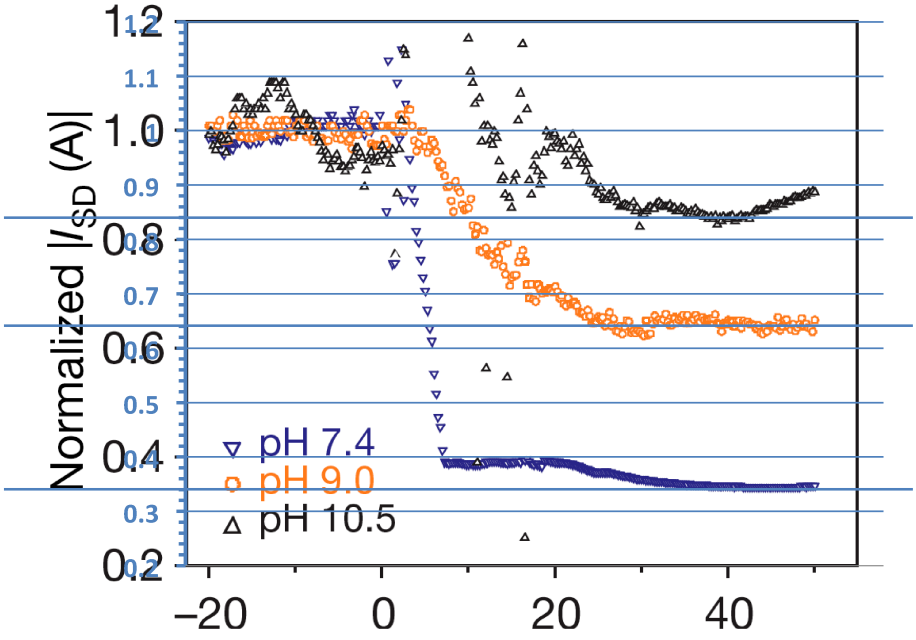

Fig. 5S Figure 2b of Ref. 27, with a superimposed grid, in order to extract experimental data.

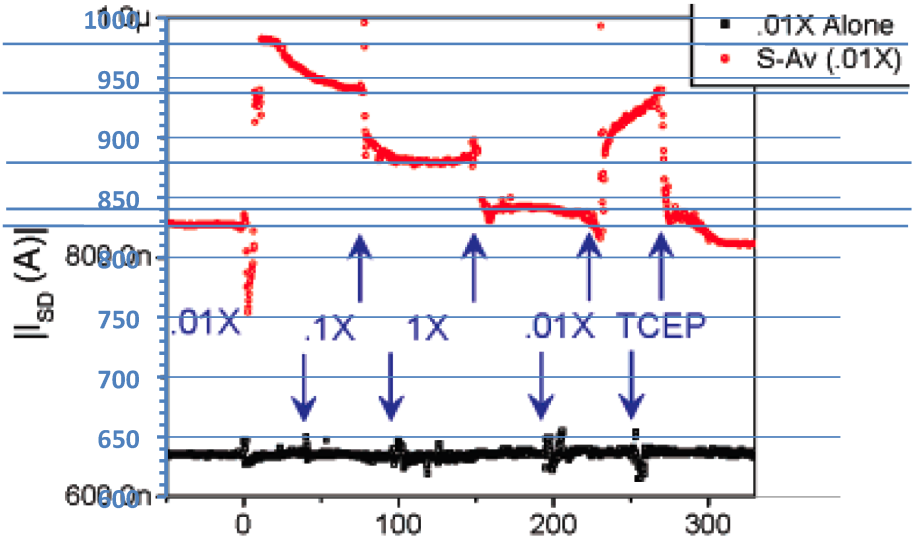

Fig. 6S Figure 3b of Ref. 25, with a superimposed grid, in order to extract experimental data. The extracted data are the red dots, together with their respective error bars, as the others represent the presence in solution of ATP and the antagonist Gleevec.

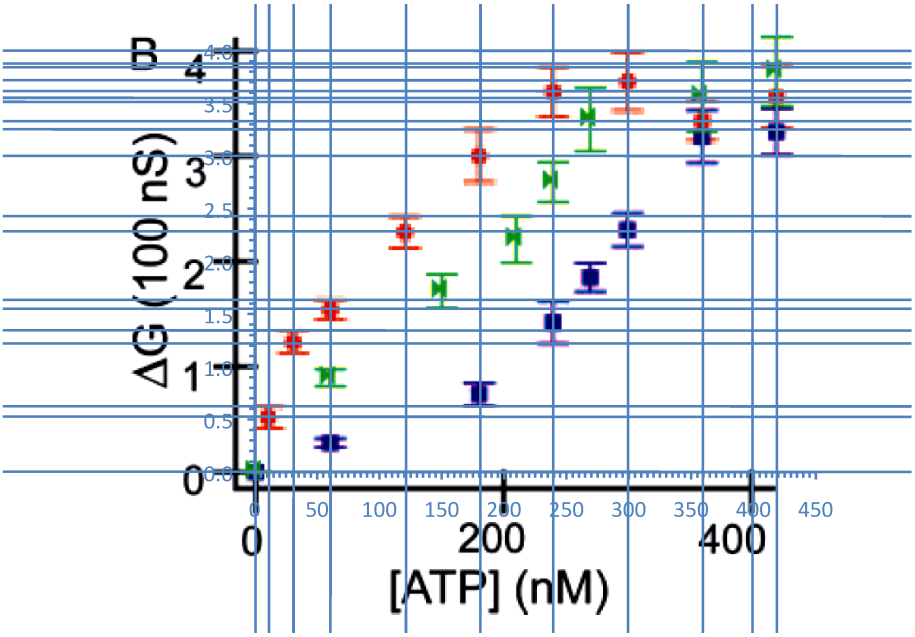

Fig. 7S Sensitivity of the ABL setup with respect to various experimentally modifiable parameters of Equations (2), (1) and (3). The sensitivity of the simulated nano-wire, as described in Section 3.4, is computed for different values in the range $\pm 20\%$ of the experimental setup, and the ensemble of results is reported against the a) nano-wire radius R, b) the nano-wire oxide layer thickness ΔR, c) the nano-wire permittivity ε_1, d) the nano-wire oxide layer permittivity ε_2 and e) the buffer Debye length λ_D. f) Sensitivity of the same nano-wire for smaller values of the buffer Debye length. In all calculations the charge density was kept fixed $\sigma_b \approx -3.1864\text{E}^{-3}$ C m^{-2}.

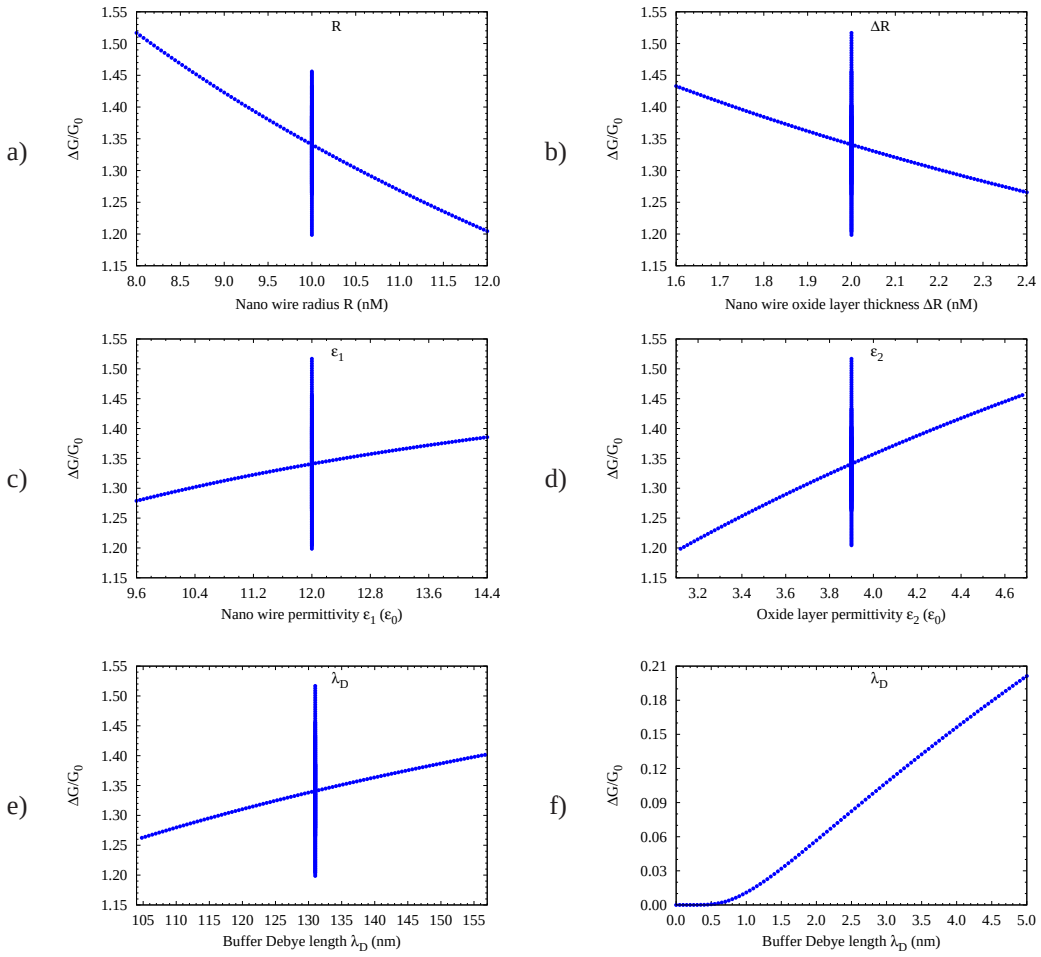

Fig. 8S Fitting of the data from Fig. 6S†. The function to fit is: $signal([\mathrm{ATP}]) = a\frac{[\mathrm{ATP}]}{[\mathrm{ATP}]+b}$. From a saturation curve fit ($f(x)$, Fig. 9S†) and from a double reciprocal fit ($g(x)$, Fig. 10S†) the parameters values are: $a = 4.56$, $b = 97.9$ and $a = 3.96$, $b = 69.8$, respectively.

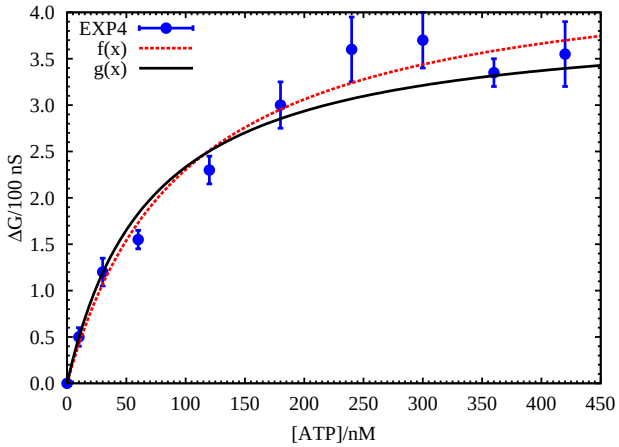

In their paper Wang et al. analyze only the linear response part of the curve and give a value for K_D of 50 nM. The experimental data is fitted to a function $f(x) = a\frac{[\mathrm{ATP}]}{[\mathrm{ATP}]+b}$, where the parameter a takes into account the signal when all available sites have been occupied, while the parameter b stands for the dissociation constant K_D. In practice, $f(x)$ is simply Equation (11), with the extra parameter a to take into account the signal values. The parameters a and b have been fitted, and their values are 4.56 and 98, respectively (Fig. 9S†). According to these fit values, the maximum possible signal registered by the devices prepared by Wang et al. would have been 456 nS. The dissociation constant of the system ABL + nano-wire with respect to the presence of ATP would have been of 98 nM. While the dissociation constant value could be plausible, the maximum possible signal seems to be too high when compared to the experimental evidence.

A somewhat more reliable fit can be obtained from the double reciprocal plot reported in Fig. 10S†. In this case, the function to fit is: $g(x) = \frac{1}{f(x)} = \frac{d}{c}\frac{1}{[\mathrm{ATP}]} + \frac{1}{c}$. With this fit, the parameter c is expected to be 3.96, which means a maximum possible signal of 396 nS, and $d = 69.8$ which gives a dissociation constant $K_D \approx 70$ nM. The two fits are reported in Fig. 8S†.

This second set of fitted parameters seems to be more in accordance with the experimental evidence. The dissociation constant is slightly larger than the experimental value of 62 nM. (A. S. Corbin, E. Buchdunger, F. Pascal and B. J. Druker, J. Biol. Chem., 2002, 277, 32214-32219) It seems more physical that the system nano-wire – ABL is less sensitive to ATP than the ABL protein isolated, which support a value for K_D larger than 62 nM. A theoretical maximum signal of 396 nS is also in line with the experimental data. It seems then a good practice to analyze eventual experimental data through the fitting of a double reciprocal plot. It allows the use of a linear fitting, while still considering the entire set of data. This practice would require the presence of more data points in the low concentrations region than what reported by Wang et al. in order for the fit to be even more precise.

It has to be noted, however, that this double-reciprocal fit (Lineweaver-Burk regression) is known to be very sensitive to data error and strongly biased toward fitting in the low-concentration range. We chose this fit since it is linear, easier and faster to compute, while still taking all the data points into account, not only the linear part, which would have been a more subjective choice.

Fig. 9S Fitting of the data from Fig. 6S as a saturation curve. The function to fit is: $f(x) = a\frac{[ATP]}{[ATP]+b}$

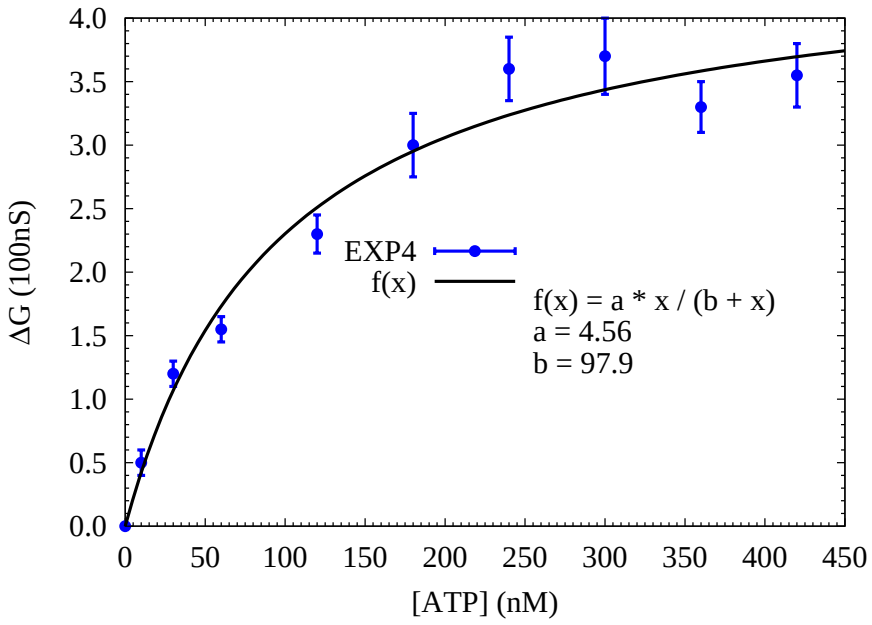

Fig. 10S Double reciprocal plot and fitting of the data from Fig. 6S. The fit function is: $g(x) = \frac{1}{f(x)} = \frac{b}{a}\frac{1}{[ATP]} + \frac{1}{a}$. With the fitted parameters, one has $a = 3.96$ and $b = K_D = 69.8$ nM.

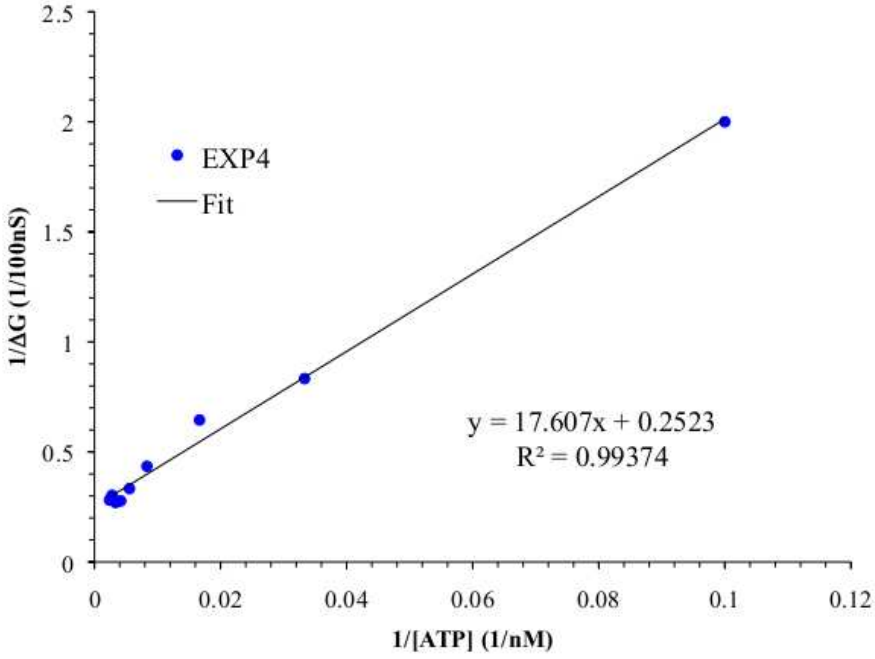

Fig. 11S Linear regression for the points in the interval 6.5 – 8.5 pH from the charge - pH curves of Fig. 4 for a) avidin and b) streptavidin.

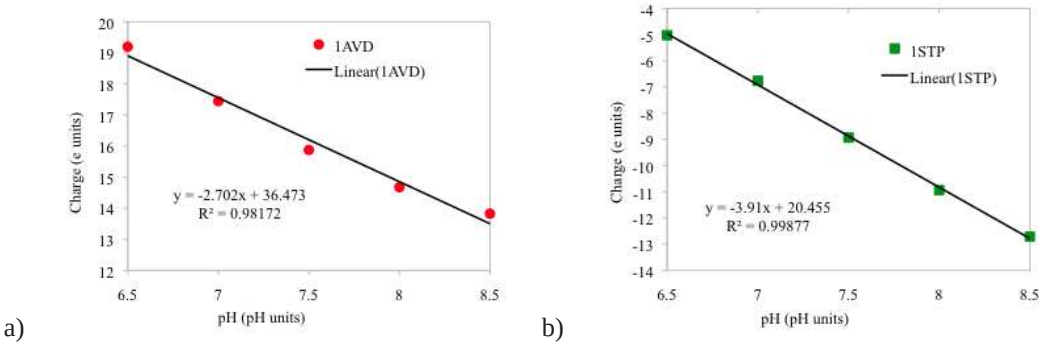

a) b)

Fig. 12S Tetrameric structure of avidin. In evidence the four equivalent chains and the four biotin molecules, one per chain. The protein is enclosed in a box of dimensions 65x65x48 Å.These are the dimensions of the parallelepiped that can be used to approximate the protein when considering the coating of the wire surface.

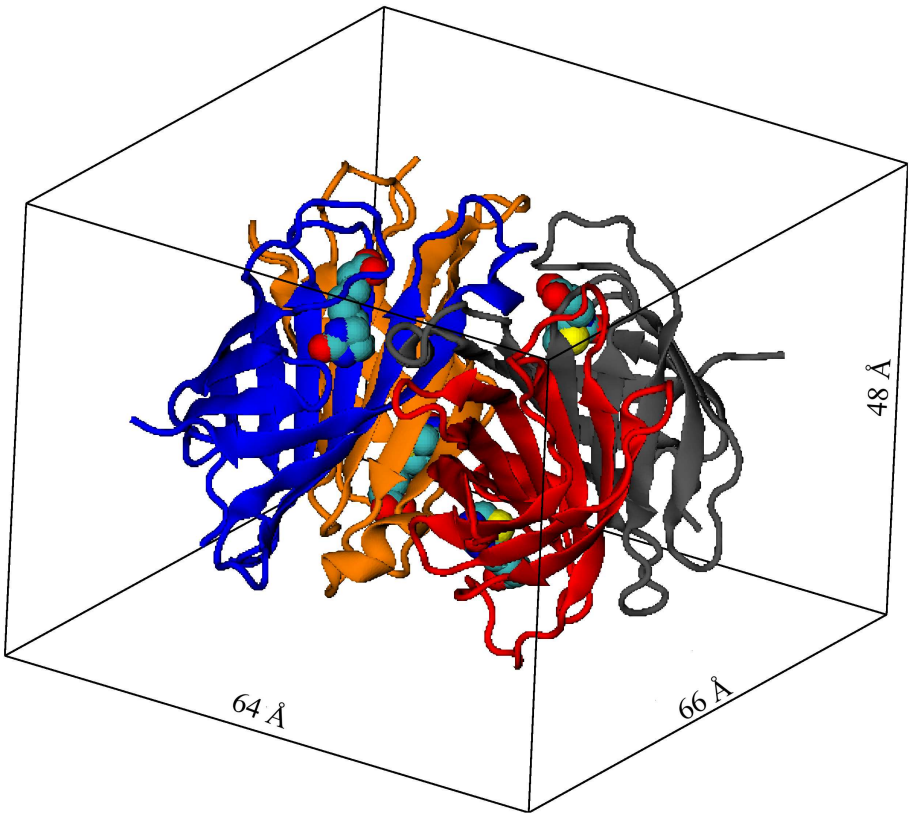

Fig. 13S Tetrameric structure of streptavidin. In evidence the four equivalent chains and the four biotin molecules, one per chain. The protein is enclosed in a box of dimensions 57x57x47 Å.These are the dimensions of the parallelepiped that can be used to approximate the protein when considering the coating of the wire surface.

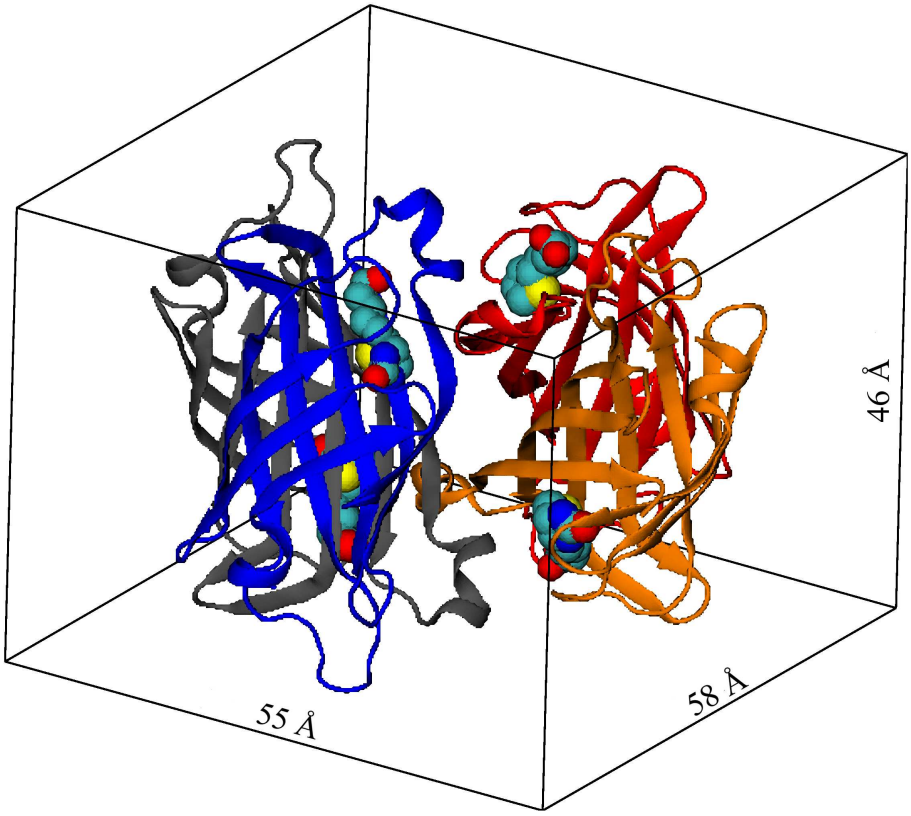

Fig. 14S The structure of ABL tyrosine kinase. In evidence the ATP molecule embedded in the protein cavity. The protein is enclosed in a box of dimensions 40x50x60 Å.These are dimensions of the parallelepiped that can be used to approximate the protein when considering the coating of the wire surface. Note that the cavity is accessible only from one of the 50x60 surfaces.

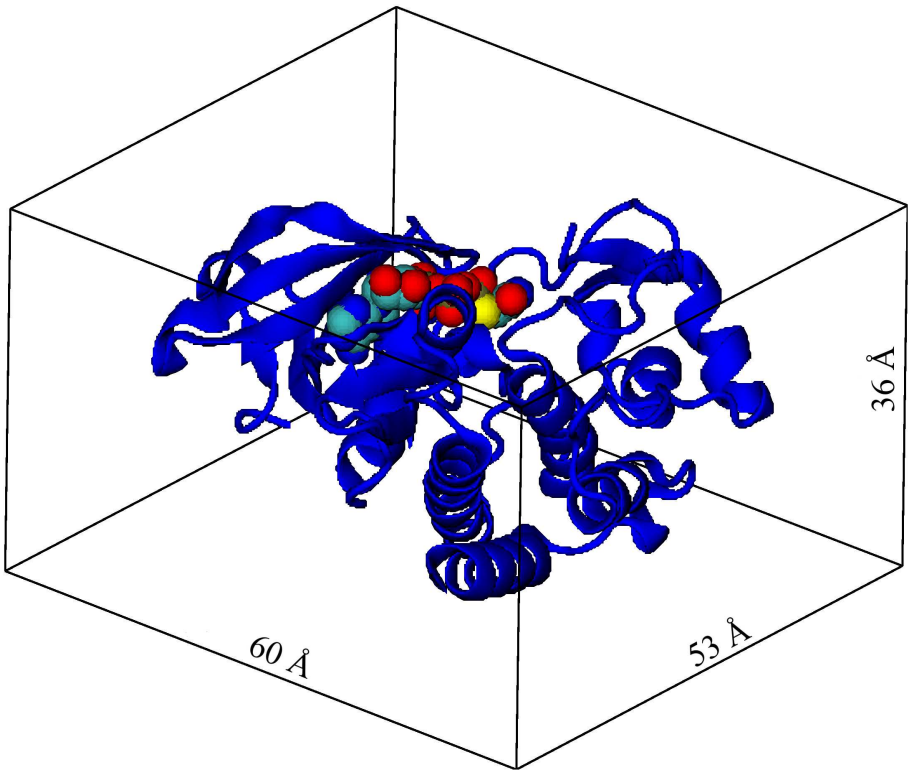

Table 1S Predicted signal change for the progressive adsorption of ATP on the standard wire, at the conditions described in Section 3.4. The ratio of adsorbed ATP depends on its concentration [ATP], following Equation (11), with dissociation constant $K_D = 62$ nM.

[ATP] (nM)	ratio	number of charges	$\frac{\Delta G}{G_0}$	ΔG (100nS)
0	0.00	0	0.000	0.00
5	0.07	102	0.102	0.28
10	0.14	189	0.190	0.53
20	0.24	333	0.334	0.93
30	0.33	445	0.446	1.24
40	0.39	535	0.537	1.50
50	0.45	609	0.611	1.70
60	0.49	671	0.673	1.88
70	0.53	723	0.725	2.02
80	0.56	768	0.770	2.15
90	0.59	808	0.811	2.26
100	0.62	842	0.845	2.36
120	0.66	899	0.902	2.51
140	0.69	945	0.948	2.64
160	0.72	983	0.986	2.75
180	0.74	1015	1.018	2.84
200	0.76	1041	1.044	2.91
250	0.80	1093	1.096	3.05
300	0.83	1130	1.134	3.16
350	0.85	1159	1.163	3.24
400	0.87	1181	1.185	3.30
450	0.88	1199	1.203	3.35
500	0.89	1214	1.218	3.39
550	0.90	1226	1.230	3.43
600	0.91	1236	1.240	3.46
∞	1.00	1364	1.368	3.81